CFD simulation benchmark on thermal-hydraulic behaviour of light metal layer

Nathalie Seiler, A. Drouillet, B. Bian, W. Villanueva, Y. Vorobyov, O. Zhabin, M. Kratochvil, L. Vyskocil

▶ **To cite this version:**

Nathalie Seiler, A. Drouillet, B. Bian, W. Villanueva, Y. Vorobyov, et al.. CFD simulation benchmark on thermal-hydraulic behaviour of light metal layer. ICONE30 - 30th International Conference on Nuclear Engineering, May 2023, Kyoto, Japan. cea-04026763

HAL Id: cea-04026763
https://cea.hal.science/cea-04026763

Submitted on 13 Mar 2023

HAL is a multi-disciplinary open access archive for the deposit and dissemination of scientific research documents, whether they are published or not. The documents may come from teaching and research institutions in France or abroad, or from public or private research centers.

L'archive ouverte pluridisciplinaire **HAL**, est destinée au dépôt et à la diffusion de documents scientifiques de niveau recherche, publiés ou non, émanant des établissements d'enseignement et de recherche français ou étrangers, des laboratoires publics ou privés.

Proceedings of the 2023
30th International Conference on Nuclear Engineering
ICONE30
May 21-26, 2023, Kyoto, Japan

ICONE30-1465

CFD SIMULATION BENCHMARK ON THERMAL-HYDRAULIC BEHAVIOUR OF LIGHT METAL LAYER

N. Seiler | **B. Bian*** | **Y. Vorobyov** | **M. Kratochvil**

A. Drouillet | **W. Villanueva**** | **O. Zhabin** | **L. Vyskocil**

CEA, DES, IRESNE
Cadarache F-13108 St
Paul Lez Durance France
nathalie.seiler@cea.fr

*KTH
Roslagstullsbacken 21
Stockholm, Sweden
**Bangor University
Nuclear Futures Institute
Bangor, UK

SSTC NRS
Vasylya Stusa St, 35-37,
Kyiv, Ukraine

ÚJV Řež, a. s.
Division 2200
Hlavní 130, Řež, 250 68
Husinec, Czech Republic

ABSTRACT

In the framework of the IAEA Coordinated Research Project on In-Vessel Melt Retention, a benchmark of CFD simulations, devoted to thermal-hydraulic behavior of the light metal layer involves several research organizations: KTH of Sweden, SSTC NRS of Ukraine, ÚJV Řež of Czech Republic and CEA of France.

This work aims at better simulating the focusing effect phenomenon leading to a heat flux peak along the height of the light metal layer, which is formed above the oxide layer in a stratified corium pool configuration during a PWR severe accident. This is a known safety issue compromising the reactor vessel integrity. The first benchmark step provides a solid foundation to the CFD schemes (physical models, meshes) by comparing the results of CFD simulations with thermal-hydraulic experimental data obtained using water as simulating fluid in a representative and quite laminar configuration. Then a similar but highly turbulent case, of higher height, is considered for more complex validation of the numerical simulation approach. Results with different turbulent models are compared against experimental data. On the strength of this encouraging work, a simulation of the same height configuration but considering steel fluid under severe accident conditions is foreseen at the final stage of this benchmark.

Keywords: Focusing effect, benchmark, BALI experiment, CFD Simulation, turbulence, Rayleigh-Bénard, DNS, RANS, LES

NOMENCLATURE

α	thermal diffusivity (m^2/s)
β	thermal expansion coefficient (K^{-1})
Cs	Smagorinsky constant
ΔT	difference of temperature (K)
ε	turbulent kinetic energy dissipation (m^2/s^3)
η	turbulent scale (m)
L	characteristic length (m)
μ	dynamic viscosity (kg/m/s)
ν	kinematic viscosity (m^2/s)
ω	turbulent dissipation rate (s^{-1})
ρ	density (kg/m^3)

1. INTRODUCTION

In the case of a hypothetical severe accident in pressurized water reactor (PWR), the melting of core materials leads to the formation of a hot magma called corium composed of oxide and metallic phases. Regarding In-Vessel Retention (IVR) mitigation strategy, these materials accumulate in the lower part of the reactor pressure vessel (RPV) and an external cooling is established to prevent the loss of RPV integrity. In standard safety studies, thermal-hydraulic research of this corium pool behavior includes lower vessel configuration cases where a molten steel metal layer forms on top of oxide corium due to the immiscibility of steel and oxides (the density of steel being lower than the density of core oxides). Past studies have confirmed that light metallic layer, heated from below by the residual power released inside the oxide layer, may produce high heat fluxes to the adjacent walls (Theerthan et al., 2020). This phenomenon is known as the focusing effect, which is considered as a major risk

© 2023 by JSME

for RPV failure in IVR strategy. A safety issue is to verify that this imposed heat flux from the metallic layer would not exceed the heat removal capability (critical heat flux) on the external surface of the vessel.

Up to now, the concept of IVR by external cooling has been investigated by several countries for different reactor designs (existing or future concepts), assuming this light metallic layer at the top of the oxide pool (Le Guennic et al, 2020). Representative experiments have been conducted to investigate this issue (BALI-metal (Bonnet and Seiler, 1999), HELM-LR for low aspect ratio (Li et al., 2021), HELM focusing on high Rayleigh numbers (Ma et al., 2015), MELAD (Theofaneous et al, 1996)) and macroscopic data (mainly**,** average temperatures and heat flux distribution) have been measured. Unfortunately, no integral test that combines relevant properties and prototypic boundary conditions is available. Furthermore, the vessel rupture is a local phenomenon and local insights are required to understand it. Therefore, we cannot rely on macroscopic simulations and more detailed (e.g., CFD) calculations are needed to demonstrate credibility of IVR strategy. Indeed, understanding the light metal layer thermal-hydraulic behavior, leading the local lateral vessel heat flux, is of primary importance. In this context, this work presents synthesised results shared by several international organizations. This work falls within the framework of the IAEA Coordinated Research Project on In-Vessel Melt Retention, which is an extension of the activities carried out previously in the frame of the H2020 IVMR project.

This work aims at better understanding the thermal-hydraulic behavior of the light metal layer to determine the local origin of the heat flux peak leading to the focusing effect. It is performed by Direct Numerical Simulation (DNS) and Computational Fluid Dynamics (CFD) thermal-hydraulic simulations. With this local investigation and understanding the focusing effect phenomenon can be modeled at a more macroscopic scale and implemented in industrial solvers such as ASTEC, PROCOR, and MELCOR (Le Guennic C. et al, 2019).

To reach this goal, as no realistic experimental results are available in prototypical conditions, a methodology based on simulations has been followed. The capabilities of the thermal-hydraulic tools and adequacy of associated meshing, models and boundary conditions choices are validated for transposed conditions (fluid, flow regimes, etc.). Since the used simulations tools are validated for conditions corresponding to focusing effect investigation studies (flows with lower Prandtl number), results of local simulations carried out in prototypical conditions are reliable. This methodology, separated in three steps of increasing complexity, has been followed by benchmark participants: the KTH Royal Institute of Technology of Sweden, the State Scientific and Technical Center for Nuclear and Radiation Safety of the State Nuclear Regulatory Inspectorate of Ukraine, The Nuclear Research Institute Rez of Czech Republic and the French Alternative Energies and Atomic Energy Commission of France.

The first step provides a solid foundation to the CFD schemes (physical models, meshing) by comparing the results of DNS and CFD simulations results with the thermal-hydraulic experimental data obtained using water as simulating fluid in a representative and quite laminar configuration. With this goal the BALI-7U test (Bonnet and Seiler, 1999) (Bonnet and Villermaux, 2001), presenting a rectangular water volume of 5 cm height with a lower heated plate and heat sink at the top and one of the lateral sides, has been selected. Then a quite similar but highly turbulent case, more consistent with developing flow in a realistic light metal layer, named BALI-8U of 40 cm height, is considered for more complex validation of numerical simulation approach. Results with different turbulent models have been compared to experimental results (DNS, LES models: Smagorinsky and WALE models) and sensitivity studies have been performed to determine best calculation schemes regarding each tool (including the simulation tool itself and associated mesh, models, boundary conditions). These two initial steps will be presented in this paper. In a near future, as these simulation tools are otherwise validated for lower Prandtl number (characteristic of light metal material), these validated calculation schemes will be applied to prototypal cases simulations to study in details the local thermal-hydraulic behavior and the related local heat transfer to the vessel surface.

In this benchmark, various simulation tools are involved: Nek5000, Fluent, ANSYS CFX and TrioCFD. Fluent, ANSYS CFX and TrioCFD are Computational fluid dynamics (CFD) tools, which numerically solve the Navier-Stokes equation. Fluent and ANSYS CFX consider variation of fluid properties (especially the density) with temperature whereas TrioCFD corrects the constant fluid density with the Boussinesq approximation, introducing a buoyancy force. ANSYS CFX and Fluent include, for treating turbulence, Reynolds-Averaged Navier-Stokes (RANS) and Large Eddy Simulation models in which either the completely turbulent spectrum or only the smallest scales are modeled, respectively. On its side, TrioCFD, in addition to RANS and LES simulations, can perform Direct Numerical Simulation (DNS) in which the completely turbulent spectrum is solved. Nek5000 is a spectral element code, which treats incompressible and low Mach-number Navier-Stokes, among others. It includes DNS, LES and RANS turbulence models.

The next section gives an overall insight on the BALI tests. Section 3 overviews the turbulence models considered in computational simulations, then section 4 describes performed work and results obtained on BALI-7U and section 5 gives first preliminary insights of works and results on BALI-8U.

2. BALI-METALTEST

The BALI-metal (BAin LIquide metal which means metallic liquid pool) program was devoted to the specific study of focusing effect phenomenon This effect appears for stratified pool configuration where metallic layer on top of oxidic pool plays a role of thermal short circuit and leads to heat flux concentration through the reactor vessel at metallic layer elevation (Bonnet and Villermaux, 2001).

2.1 Experimental apparatus

© 2023 by JSME

The test geometry is described in Figure 1. The test section is rectangular of size 0.13m in width along the axis Y, 2m in length along X and the height along the axis Z that can be adjusted depending on the specific experimental needs. The test section is filled with water and heated from the bottom by an imposed heat flux. Front and backsides and one lateral side are made of plexiglas for flow visualization and considered as adiabatic walls. The top surface and the other lateral side allow heat removal.

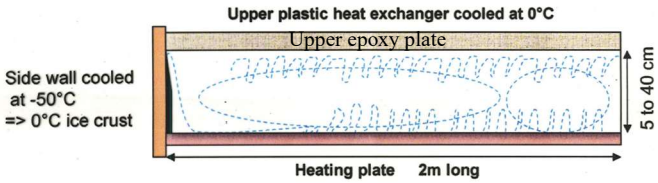

FIGURE 1: BALI-Metal experiments scheme

A heat exchanger imposes a constant 0°C boundary condition at the upper surface of the upper rigid epoxy plate of 0.41mm height and 0.41 W/m/K heat conductivity (Villermaux, 1999) (figure 2).

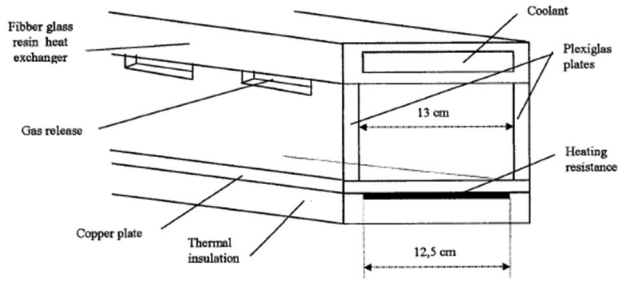

FIGURE 2: *Transverse cross-section of the BALI-Metal section*

This upper heat removal has been designed by Villermaux (Villermaux, 1999), based on a transposition method, to simulate the radiation heat transfer occurring in the real reactor case. On the lateral side, an isothermal boundary condition is reached by cooling the water and thus creating a thin ice layer of a few millimeters of thickness. It does not disturb neither the volume nor the geometry of the water pool. Tests are conducted at atmospheric pressure (1 bar).

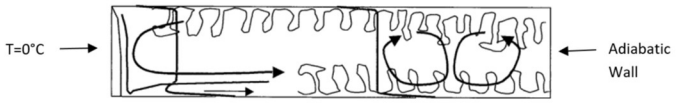

FIGURE 3: *General flow observations*

The steady-state flow behavior during these tests is drawn in figure 3. The pool is divided into two parts. On the side of lateral cooled wall, a boundary layer with a downward flow of water has been observed, influencing the bottom heated plate and spreading over it as a cold tongue. On the other side near the adiabatic wall (which simulates the axis of cylindrical geometry), the flow pattern, which is not influenced by the lateral cooled wall, is similar to observations performed in Rayleigh-Bénard convection cells. Thermal-hydrodynamic instabilities are released from heated plate as hot plumes and from upper heat exchanger as cold plumes inducing unstable convection motion at larger scale. The wavelength between plumes at hot or cold surfaces are about 1 cm. As these plumes control the heat transfer, it was concluded (Bonnet and Villermaux, 2001) that a 13 cm thickness of test section is large enough to have several developed plumes and be representative of the heat transfer mechanism in reactor case. Along with the increasing distance from the cooled wall, the cold tongue thickness and its temperature gradually increase whereas its velocity decreases up to a location where thermal-hydrodynamic instabilities are no longer blown away and are strong enough to appear at the surface of the heated plate. The flow is fluctuating in the pool. Large-scale convection cell induced by lateral cooling over the whole test section periodically breaks into several unstable smaller scale convection cells induced by thermal-hydrodynamics instabilities. The period between these two flow regimes (large scale convection and Rayleigh-Bénard instability) depends on the height of the layer. Temperature measurements allow to estimate this period (Bonnet and Villermaux, 2001). Measurements enable to get global power balance on the section surfaces, some temperature profiles and some features of the flow structures (plumes period, length of the cold tongue).

One major conclusion from this experimental work was that the decrease of the pool height results in a greater suppression of the large scale convection induced by the lateral cooling and thus the radial temperature gradient increases. The reduction of the heat flux concentration factor (focusing effect) is thus observed for layer thickness smaller than 20 cm; this reduction is limited to -25% for a thickness of 5 cm. This effect is related to the apparition of a radial thermal gradient in the pool and cannot be described by a simple 0D approach. Furthermore, due to convective mixing, the heat loads profile (imposed on the bottom surface) has only a very weak effect on radial temperature gradient in the fluid layer and consequently on the heat flux concentration factor.

Moreover, from the BALI-Metal test campaign, correlations of average Nusselt numbers on the upper and lateral cooled surface have been established depending on the Rayleigh number. From transposition considerations, these correlations in rectangular 2D geometry have been adapted to cylindrical 3D geometry. But following this approach, the average heat fluxes over the surfaces are obtained at larger scale (macroscopic scale) than the ones that can be obtained by CFD calculations (local scale).

2.2 Experimental matrix

The main adjustable parameter is the height of the water layer. Four different heights have been investigated in the BALI-Metal campaign: 5, 10, 20 and 40 cm. The second parameter is the heat flux profile provided to the bottom layer. Observations of upward heat transfer in oxide pool in the frame of COPO or BALI facility (Bonnet and Seiler, 1999) show that upward heat flux is uniform. Nevertheless, in MVITA calculations, some

© 2023 by JSME

local corner effect has been observed (Bonnet and Villermaux, 2001). In the vicinity of the vessel, the oxide crust is thicker and consequently the heat flux injected in the metallic layer is locally lower. To take into account this effect, two different heat flux profiles have been tested

- Uniform profile
- Non uniform profile: null power on the first area (vicinity of lateral cooled wall) and then a uniform profile.

In the context of this benchmark, in order to converge on CFD schemes, only cases with uniform heating have been selected. Among the conclusions of the former project on IVMR achieved in the Horizon 2020 European Program (Carénini et al., 2020), the influence of boundary conditions (especially upward radiation and lateral heat losses) was highlighted for the simulation of such a light metal layer as well as the required accurate modeling of turbulent flow. In these IVMR conclusions, the non-representativeness of water (with high Prandtl number) laminar experiments for light metal layer thermal-hydraulics presenting low Prandtl number was also raised. Indeed, a low Pr can lead to a more turbulent flow and more even redistribution of heat (Bian et al., 2022). However, the turbulent effects would disturb the large-scale convective cells due to the lateral cooled wall. Moreover, having validated the CFD schemes in water, results obtained with this methodology should be representative in steel flow because domain of low Prandtl numbers is integrated in the CFD tool validation matrix. In the continuity of these first IVMR achievements, it is proposed within the framework of the IAEA Coordinated Research Project on In-Vessel Melt Retention to lay and agree on solid CFD schemes foundations on a laminar case (5cm height) and then to simulate a turbulent case of higher height (40cm). A 2kW power is injected at the bottom in both selected tests:

- The low height test is BALI-7U of 5cm height. Furthermore, results of the reproducibility test BALI-6U in the same conditions are added to this benchmark.
- The high height test is BALI-8U of 40cm height

2.2 Flow features

Regarding the construction of the CFD schemes (related to each CFD tool used), first technical exchanges within the benchmark were on the turbulence and models. The non-dimensional numbers (Prandtl, Grashof and Rayleigh) characteristic in both tests are reported in table 1.

The Rayleigh number is around 7×10^7 in BALI-7U and 2×10^{10} in BALI-8U. As already discussed, the global flow behavior is influenced on one side by Rayleigh-Bénard instabilities induced by bottom heating and upper cooling and on the other side by the large-scale convection cell induced by lateral cooling. The Rayleigh-Bénard instabilities have more influence as the proportion of heat evacuated by the top is important in regard to the one evacuated laterally. This is the case for the low height test BALI-7U (85% of the injected bottom heat flux is removed by the top compared to 41% in the BALI-8U case (Bonnet and Villermaux, 2001)).

In a first approximation, if only Rayleigh-Bernard instabilities are considered, past R&D researches place BALI-7U in the 'soft turbulence' regime and BALI-8U in the 'hard turbulence' regime (figure 4) (De et al., 2017).

Parameter	Formulation/Estimation	BALI_7U value	BALI_8U value
L	Characteristic length (height)	0.05m	0.4m
ΔT	Temperature difference	56K	33K
Pr	$\frac{\nu}{\alpha}$	6.943	6.943
Gr	$\frac{g\beta\,\Delta T\,L^3\rho^2}{\mu^2}$	1.030×10^7	3.107×10^9
Ra	$Gr.Pr$	7.149×10^7	2.157×10^{10}
Nu	$0.05Ra^{1/3}$	20.75	139.18
Re	$0.088Ra^{4/9}Pr^{-2/3}$	717.89	9080.25
η_K	$\frac{Pr^{1/2}L}{Ra^{1/4}\,(Nu-1)^{1/4}}$	6.80×10^{-4}m	8.02×10^{-4}m
η_B	$64\times0.482^4\times0.982^6\times Nu^5Ra^{-1}\eta_K$	4.34×10^{-4}m	1.33×10^{-3}m

* Estimated according to S. Grossmann and D. Lohse (2000) – Diagram, area IV_u.
** Estimated according to O. Shishkina (2010).

TABLE 1: *General flow features and non-dimensional numbers*

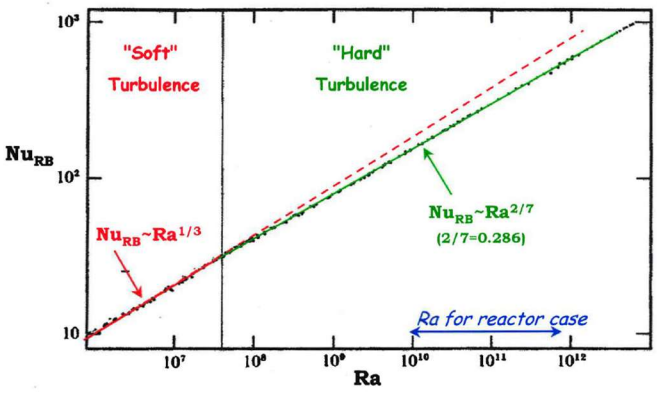

FIGURE 4: Scaling of hard thermal turbulence in Rayleigh-Bénard convection (Castaing B., et al., 2006)

This leads to the conclusion that BALI-7U is not highly turbulent whereas BALI-8U is. This statement applies the need of turbulence models and adequate related meshes for BALI-8U. Furthermore, assuming once more the predominance of Rayleigh-Bénard instabilities, Grossmann and Lohse (Grossmann and Lohse, 2000) established a method to estimate, for natural convective flows, the equivalent Reynolds number and the associated turbulence scales in Rayleigh-Bénard configurations necessary for the realization of adequate meshes in regard to turbulent models. The equivalent Reynolds number of ~700 obtained in BALI-7U confirms the laminar behavior of this flow and of 9×10^3 in BALI-8U confirms the turbulent regime (table 1).

An order of magnitude of the Kolmogorov (η_K in table 1) and Bachelor length scales (η_B in table 1) could be derived. Kolmogorov length scale expresses that the smallest turbulent

© 2023 by JSME

scale is governed by the viscous under-layer whereas in case of Bachelor length scale, the dominant scale is the one related to the diffusion phenomenon. The minimum mesh size should be less than the Taylor scale, which, in classical hydrodynamic turbulence, is greater than the Kolmogorov length scale to solve the completely turbulent spectrum with DNS method. This scale is found to be ~0.4mm in BALI-7U and ~0.8mm in BALI-8U. But as, not only Rayleigh-Bernard instabilities govern the global flow behavior, 2D preliminary DNS (highly meshed) simulations have been performed with TrioCFD and these length scales have been statistically estimated from velocity fluctuations. In BALI-7U, consistent values of $\eta_K = \nu^{3/4}\varepsilon^{1/4}$ ~ 1.1 mm and of $\eta_B = \left(\frac{\nu}{\varepsilon}\alpha^2\right)^{1/4}$ ~ 0.45 mm have been obtained confirming the previous orders of magnitude even in case of the combing effects on the global flow (Rayleigh- Bénard and cooled wall). Likewise for BALI-8U, η_K~ 2.7 mm and η_B~1 mm are consistent with table 1.

3. TURBULENCE MODELS

On the strength of these investigations, each benchmark participant has considered adequate meshes regarding their selected turbulence models.

Among the RANS approaches for which all turbulent fluctuations are modelled, the Shear Stress Transport (SST) model is considered (Menter, 1994). There is a two-equation eddy viscosity model which combines the k- ω turbulence model and k- ε turbulence model such that the k- ω is used in the inner region of the viscous boundary layer and switches to the k- ε in the free shear flow; ε being the turbulent kinetic energy dissipation and ω the turbulent dissipation rate.

Large Eddy simulations provide a very promising approach for the simulation of turbulent flows because of quite lower computation times than those of DNS. Further, their resolution of turbulent structures is more accurate in comparison to Reynolds Averaged Navier–Stokes (RANS) simulations; scales upper than Taylor are directly resolved (in DNS) and lower are modeled (figure 5).

In LES simulations, an additional viscosity, called the turbulent eddy viscosity ν_T, is introduced in order to model the turbulence. This eddy viscosity is given by:

$$\nu_T = (C_S\Delta)^2|\tilde{S}| \qquad (1)$$

where Δ is the effective grid scale, and $|\tilde{S}|$ derived by Smagorinsky (Smagorinsky, 1963) exclusively from the shear stress tensor. It is the magnitude of the filtered strain rate tensor. Further assumptions among which that the cutoff wavenumber is in the inertial subrange of a Kolmogorov-type spectrum, lead to a constant Cs between 0.05 and 0.18. However, the eddy viscosity remains positive even in laminar flows where it should tend to zero. Moreover, it was shown by Nicoud (Nicoud and Ducros, 1999) that in Smagorinsky's formulation, the wall boundary law is not fulfilled. The eddy viscosity neither does not tend to zero. The Cs constant is by default 0.1 in ANSYS CFX and Fluent and is 0.18 in the Smagorinsky model implemented in TrioCFD.

In the Smagorinsky–Van Driest model (Lilly, 1992), the LES model constant Cs follows an exponential law depending of the non-dimensional distance (y+) to the wall. This extended Smagorinsky model gives a more precise description of the wall boundary layer (Nicoud and Ducros, 1999). One disadvantage of this approach is the global dependence of the damping function on the dimensionless wall distance. Finally, the WALE model (Nicoud and Ducros, 1999) is based on the square of the velocity gradient tensor, which takes into account not only the shear stress tensor but also the rotation tensor. In this case, in addition to the constant of Smagorinsky (0.18 in TrioCFD), a new constant is included. This method enables to simulate more realistically the turbulent flow behavior near the wall without dynamical algorithms or damping functions.

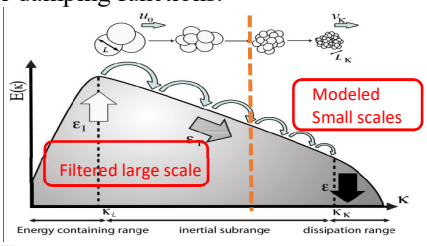

FIGURE 5: Sketch of the energy cascade (Sagaut, 2016)

Finally, most predictive turbulent simulations are direct numerical simulation (DNS) in which the Navier–Stokes equations are numerically approximated without any turbulence model. This means that the whole range of spatial and temporal scales of the turbulence must be resolved (figure 5).

4. BALI-7U INVESTIGATION, RESULTS AND DISCUSSION

The upper boundary condition of test BALI-7U has been discussed between the benchmark participants.

4.1 Upper boundary condition

From the experimental report (Bonnet and Villermaux, 1999), the fluid inside the test section was cooled by coolant at 0°C flowing inside the upper plastic/epoxy heat exchanger (see Figure 2). Bonnet and Villermaux reported that the upper epoxy surface (of the lower plate of the heat exchanger) was uniformly cooled at 0°C. They measured the equivalent resistivity between the fluid at the highest location inside the test section and the fluid inside the coolant as 0.01 m^2·K/W. Furthermore, the heat balance given from experiment was closed: 15% of the injected power lost by the cooled side and 85% by the upper surface.

From this experimental evidence, the modeling strategy of each participant has differed. These choices are displayed in figure 6.

CEA has simulated the real configuration, with the heat conduction inside the lower epoxy plate of thickness 4.1mm and conductivity 0.41 W/m/K (configuration A-fig 6) and verified that results are the same as the ones obtained in configuration B, where an equivalent heat transfer of 100 W/m^2/K is directly applied between the lower surface of this epoxy plate and the fluid in the heat exchanger. KTH has also computed this heat

© 2023 by JSME

exchange imposing directly such convective heat coefficient between the lower epoxy plate and a 0°C boundary condition. In other tests, a convective heat coefficient of 135 W/m²/K has also been considered by CEA and KTH to be consistent with the strategy of SSTC NRS and UJV (see next).

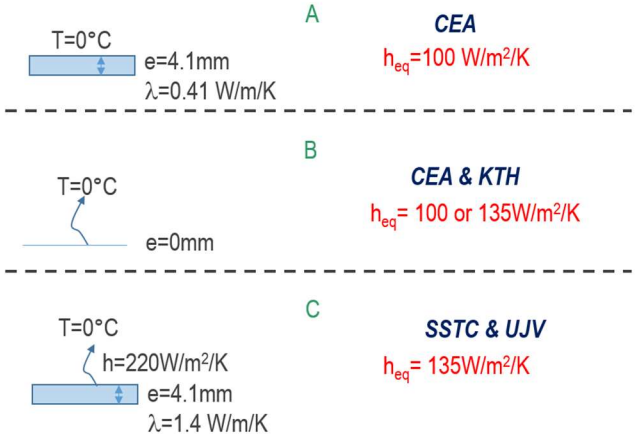

FIGURE 6: Sketch of the heat transfer in the lower epoxy plate of the upper heat exchanger - The lower epoxy plate of the upper heat exchanger is displayed in blue.

Indeed, from temperature measurements, given in the benchmark, SSTC NRS derived a convective heat coefficient of 220 W/m²/K between the upper side of the epoxy plate and a 0°C boundary condition given by the flowing fluid inside the heat exchanger. This value of 220 W/m²/K, is explained by the higher value of epoxy conductivity considered in their conduction model (coupled to the thermal-hydraulic model). But, by looking closer, it can be observed that the resulting equivalent heat transfer coefficient (between the upper surface of the fluid and the 0°C boundary condition) is h_{eq}=135 W/m²/K close to 100W/m²/K.

4.2 Simulation cases

Finally, the simulations carried out during this benchmark on the BALI-7U case are given in table 2.

Participant (tool)	*Equivalent upper heat coefficient (W/m²/K)*	*Turbulence model*
ÚJV Řež (Fluent)	135	LES Smagorinsky with Cs=0.1
		LES Smagorinsky with Cs=0.05
SSTC NRS (ANSYS CFX)	135	LES Smagorinsky with Cs=0.1
		RANS SST
		None (~ laminar)
KTH (Nek5000)	100	DNS
	135	DNS
CEA (TrioCFD)	100	None - Adapted mesh→DNS
	135	None Adapted mesh→DNS
		LES WALE

TABLE 2: *Performed simulations of BALI-7U (not presented results are in italic)*

As the results are oscillatory in time (even when the steady state is reached as explained in the section 2), results are time-averaged for 50min (as in the experimental procedure) and the mean and the standard deviation are computed (and thus maximum and minimum values). Global average computing information is given in table 3.

	CEA TrioCFD	UJV FLUENT	SSTC NRS CFX	KTH Nek5000
Mesh size	9.3 10^6	1.7 10^6	6.7 10^5	20m grid points
~CPU time	10 days	1 month	17 days	

TABLE 3: Global average computing information

4.3 Results and discussions

Available experimental temperature and heat flux profiles have been compared as well as global data. Results of simulations presented in table 2 are plotted in the following figures except the SSTC-NRS RANS-SST case, which gave temperature profiles in agreement with experiment but underestimated the removed lateral power and the CEA LES WALE model, which gave similar results as the same CEA case without turbulence model.

In figures 7, 8, and 9, profiles of the mean temperatures along X at the top, middle height and bottom of the fluid domain are displayed. The average range of temperature fluctuations is given in table 4.

General conclusions are that simulations results are consistent whatever the way to impose the upper condition for a same equivalent heat coefficient. Simulations results with h_{eq}=135 W/m²/K give closer results to experimental temperature profiles than with the value of 100W/m²/K recommended by the experimental report. Results are more dispersed at the bottom location and globally over-estimate measured temperature at the adiabatic wall side. This can come from some possible experimental heat losses on this side which were not taken into account in the simulation boundary conditions.

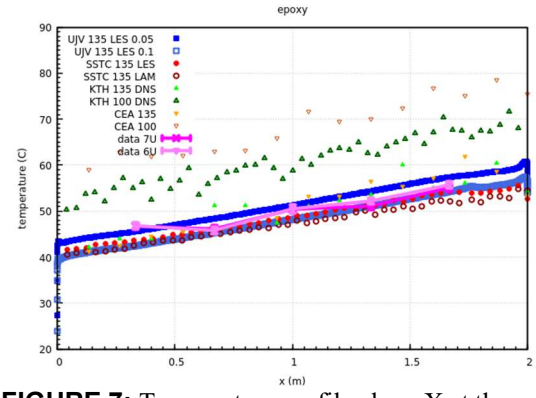

FIGURE 7: Temperature profile along X at the epoxy plate (at the middle width Y). The cooled wall location is X=0m.

© 2023 by JSME

Moreover, it appears that in this BALI-7U test, turbulent and laminar simulations give quite similar results regarding the temperature profile along X. This is underlined also in the lateral temperature (X=20cm) and heat flux profile along the cooled wall. In figure 10, for h_{eq}=135 W/m^2/K, temperature profile is well simulated by laminar simulations and turbulent LES simulations considering the Smagorinsky model with the lowest constant Cs=0.05 and, thus, for which the eddy viscosity is very small.

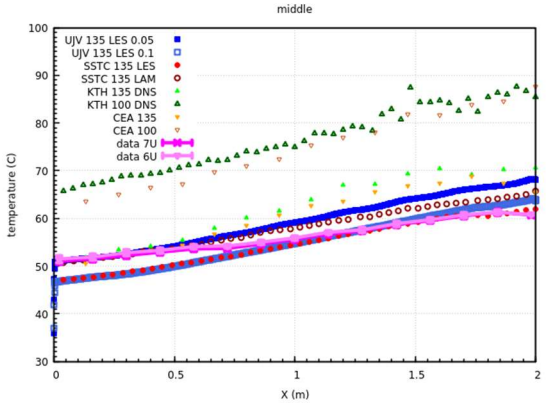

FIGURE 8: Temperature profile along X at the middle height Z (at the middle width Y). X=0m at the cooled wall.

On the contrary, results with the Smagorinsky model with a higher constant Cs=0.1 underestimate the experimental profile. More differences are observed in the localizations close to bottom plate, corresponding to the simulation of the cold tongue. Further investigations on this point are foreseen.

Finally, the results for the heat flux profile along the cooled wall are displayed in figure 11 and present good agreement together and with the adjusted experimental data (to conserve the overall power evacuated on this wall experimental data being subject to errors due to conduction in the lateral plate where measurements were made (Bonnet and Villermaux, 1999)).

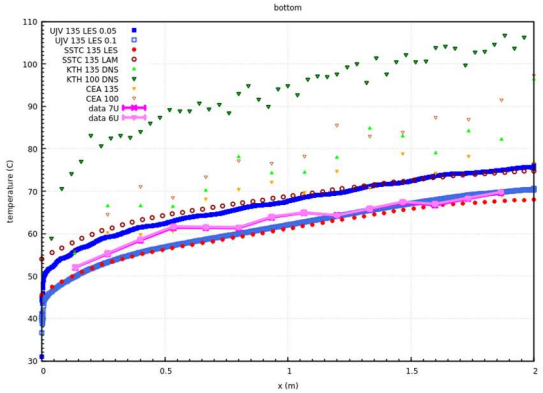

FIGURE 9: Temperature profile along X at the bottom on the heated plate (middle width Y). X=0m at the cooled wall.

DNS results from KTH and CEA (laminar with adapted fine mesh to turbulence scales) results at h_{eq}=135 W/m^2/K remain close to unadjusted data.

Average variables (temperature, heat flux) are reported in tables 4 and 5 and compared to experimental data. Regarding DNS results, simulations with h_{eq}=100 W/m^2/K better agree with experimental results. The fact that in DNS, temperatures are close to experimental values with h_{eq}=135 W/m^2/K whereas heat fluxes are better simulated with h_{eq}=100 W/m^2/K could be explained by the non-negligible heat losses on the supposed adiabatic walls in the case with h_{eq}=100 W/m^2/K. It is worth noting that lateral removed heat flux is the main variable of interest for focusing effect issue. Heat losses are compensated taking h_{eq}=135 W/m^2/K that is why global temperature level is consistent in this case.

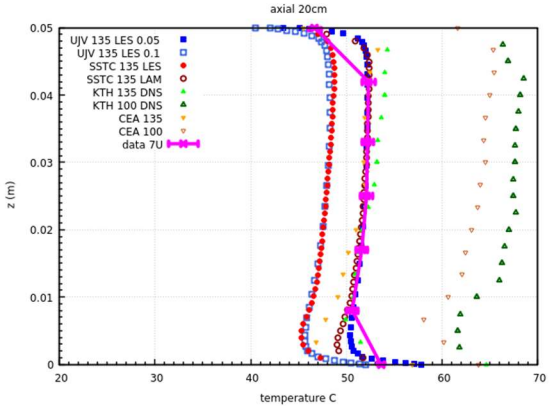

FIGURE 10: Temperature profile along the height Z, at X=20cm (at the middle width).

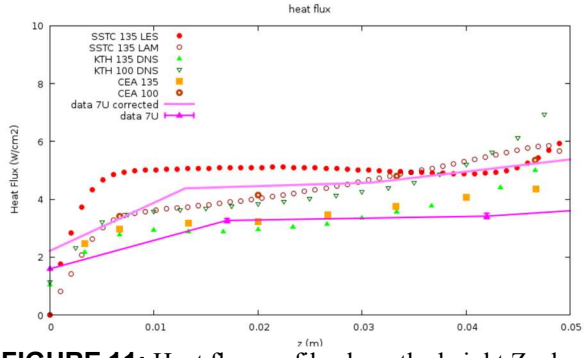

FIGURE 11: Heat flux profile along the height Z, along the cooled wall at X=0cm (at the middle width)

		CEA		UJV		SSTC		KTH	
cas	exp	100	135	135 Cs 0.05	135 Cs 0.1	135 LES	135 LAM	100 DNS	135 DNS
T middle (°C)	**56.3**	73	**60.2**	**59.3**	61.3	**53.6**	**56.9**	76.4	**58.9**
T up (°C)	49.8	69	51.3	51.6	45.6	47.8	46.6	65.4	48.1
T down (°C)	62.8	77	68.6	67	65	60.3	67.8	86.4	71.2
deviation (°C)	0.3-0.8	1.3-4.7	2.1-5.2	1.3-2.69	0.3-2.9	1.09-4.14	1.1-5.57		

© 2023 by JSME

TABLE 4: *Comparison of average (over the X plane) temperatures in BALI-7U*

Thus consistent results between experimental and simulation results are shown in tables 4 and 5 as well as the variability on the concentration factor (Φ_{lat}/Φ_{down}).

		CEA		UJV		SSTC		KTH	
cas	exp	100	135	135 Cs 0.05	135 Cs 0.1	135 LES	135 LAM	100 DNS	135 DNS
Φ up (W/cm²)	-0.65	-0.64	-0.66	-0.68	-0.64	-0.65	-0.65	-0.65	-0.68
Φ down (W/cm²)	0.77	0.77	0.77	0.8	0.8	0.77	0.77	0.77	0.77
Φ left (W/cm²)	**-4.54**	-4.9	-3.6	-4.7	-5.1	-4.6	-4.3	-4.46	-3.18
Concentration factor	**5.90**	6.36 7.8%	4.67 -25.9%	6.1 3.4%	6.62 12.2%	5.97 1.2%	5.58 -5.4%	5.79 -1.9%	4.12 -30%

TABLE 5: *Comparison of heat fluxes in BALI-7U*

In conclusion, of BALI-7U benchmark, the numerical simulations are in good agreement with experimental results especially for simulations with low turbulence. This validates our reflections on the flow behavior characterization and the methodology for realistic simulation results (boundary conditions choices, meshes, turbulence models).

5. BALI-8U INVESTIGATION, RESULTS AND DISCUSSION

This methodology has been applied to the BALI-8U case. Turbulence length scales have been evaluated (§3) and meshes have been realized accordingly.

5.1 Boundary conditions and Simulation cases

Once again, the boundary conditions have been discussed because in the experimental report (Bonnet and Villermaux, 1999) the heat balance given from experiment was: 43% of the injected power lost by the cooled side and 41% by the upper surface. The remaining 16% should be lost on front, back and right lateral sides. Various boundary conditions have been envisaged.

- SSTC NRS based on experimental temperatures, simulates the upper heat convection in the exchanger with a coefficient of 170 W/m²/K, which corresponds to an upper equivalent heat coefficient between the upper surface of water and the 0°C boundary condition of 113 W/m²/K. Furthermore, heat losses on the lateral walls are simulated considering a heat transfer coefficient of 14.8 W/m²/K and a boundary temperature of 20°C. It corresponds to the 16% of lost power (~322 W). This way of modelling of the boundary condition is called BC1 (figure 12).
- CEA starts with the preliminary boundary conditions for which the energy balance is not closed (h_{eq}=100 W/m²/K and no lateral losses). This boundary condition is called BC0. Then, same boundary conditions as of SSTC NRS (BC1) are considered, for comparison purpose, but imposing directly the heat fluxes on lateral wall as a Neumann condition).
- ÚJV first keeps the same modeling of the upper condition as in BALI-7U (resulting in h_{eq}=135 W/m²/K) and adds the lateral losses on the left lateral surface only (while the right lateral surface remains adiabatic). Heat conduction in a plexiglas thickness of 0.01m (conductivity of 0.18 W/m/K) is explicitly considered and then a heat convective coefficient of 7 W/m²/K in the air associated to a boundary temperature of 21°C is applied. This leads to a deducted lateral heat flux of 67.9 W/m². This initial modelling approach applied by ÚJV is called BC2. Finally, as the removed lateral heat was too low the lateral heat convective coefficient was increased to 109.2 W/m². That boundary condition is called BC3 and leads to a global lateral power loss of 174 W (only 8% of the injected power compared to 16% in the experiment).

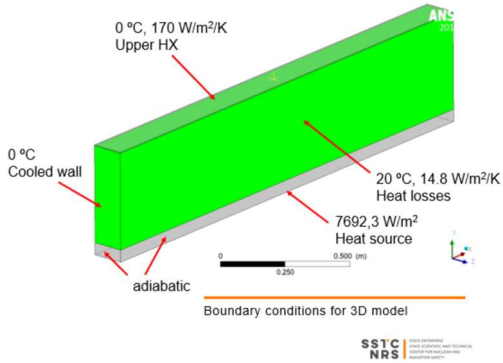

FIGURE 12: Boundary conditions in BALI-8U considered by SSTC NRS. h_{eq}=113 W/m²/K.

Finally, the simulations carried out during this benchmark on the BALI-8U case are given in table 6. Corresponding DNS calculations are ongoing.

Once again, as the results are oscillatory in time, results are time-averaged for 180min. Global average computing information is given in table 7.

Participant (tool)	*Boundary condition*	*Turbulence model*
ÚJV Řež (Fluent)	BC2	LES Smagorinsky with Cs=0.05
	BC3	
SSTC NRS[1] (ANSYS CFX)	BC1	LES Smagorinsky with Cs=0.1
		LES WALE
CEA (TrioCFD)	BC0	LES WALE
		RANS k- ε

[1] Converged results have only been averaged on 1100s and are still going on

© 2023 by JSME

	BC1	LES WALE[2]
		RANS k- ε

TABLE 6: *Performed simulations of BALI-8U*

	CEA (TrioCFD)	UJV (FLUENT)	SSTC NRS (CFX)
Mesh size	20 10^6 (LES) 1.4 10^6 (RANS)	11 10^6	8.3 10^5
~CPU time	0.5-1 month	1 month	1.5 month

TABLE 7: Global average computing information

5.2 Results and discussions

In figures 13, 14, and 15, profiles of the mean temperatures along X at the top, middle height and bottom of the fluid domain are displayed.

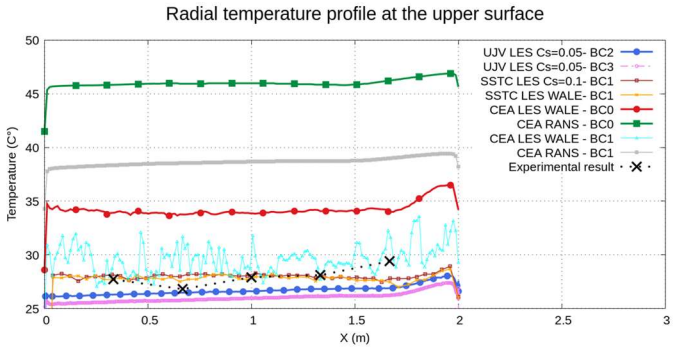

FIGURE 13: Temperature profile along X at the upper epoxy plate. The cooled wall location is X=0m.

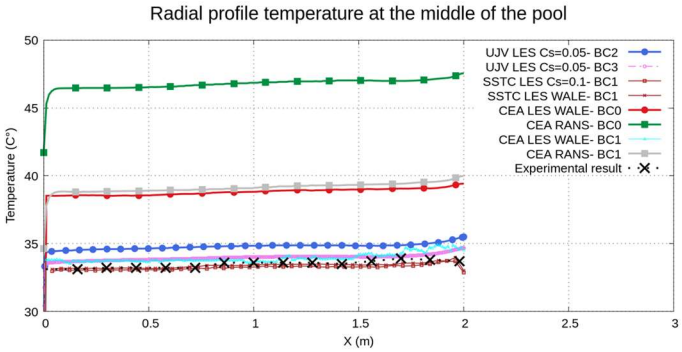

FIGURE 14: Temperature profile along X at the middle of the pool height. The cooled wall location is X=0m.

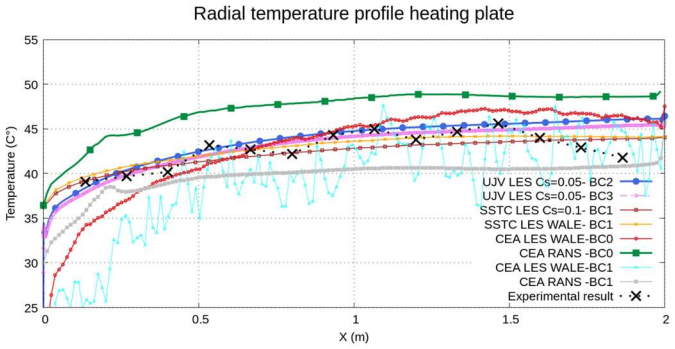

FIGURE 15: Temperature profile along X at the bottom plate. The cooled wall location is X=0m.

Regarding the boundary conditions, as expected with BC0, BC2 and even BC3 conditions, for which the energy balances in the pool in not closed (even in BC3 where 8% of injected power is not released), the temperature is generally over-estimated, even though BC2 and BC3 (with LES Smagorinsky model Cs=0.05) slightly under-estimate the temperature radial profile at the upper surface. BC1 condition (corresponding to a closed energy balance) gives the best results. Concerning the turbulent models, even with this BC1 condition, the RANS k-ε still largely over-estimate the temperatures. CEA results show that, with the same boundary condition, LES WALE model leads to lower radial temperatures profiles than RANS model. LES WALE and Smagorinsky model applied with BC1 (with a high Cs value of 0.1, characteristic of developed turbulent flows) give similar results, which are very close to the experimental data. These conclusions are confirmed by axial temperature at 33 cm and heat flux profiles along the cooled wall (figure 16 and figure 17). This heat flux profile is well reproduced by LES models (still under calculation for averaging) whereas RANS simulations give flat profiles. These results are under investigation.

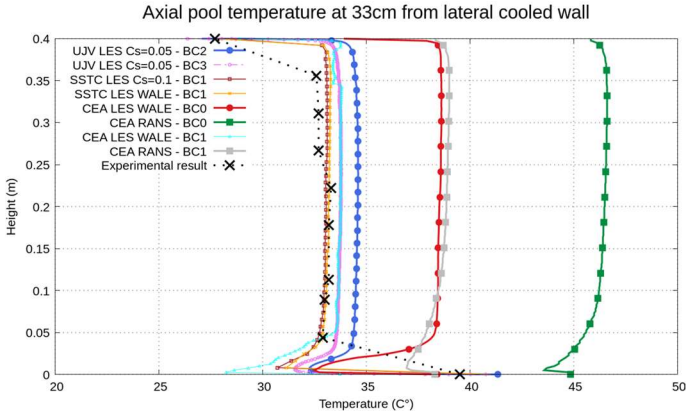

FIGURE 16: Temperature profile along Z at X=33cm.

[2] Results are snapshot at 2020s when results are already converged. Simulations are still going on.

© 2023 by JSME

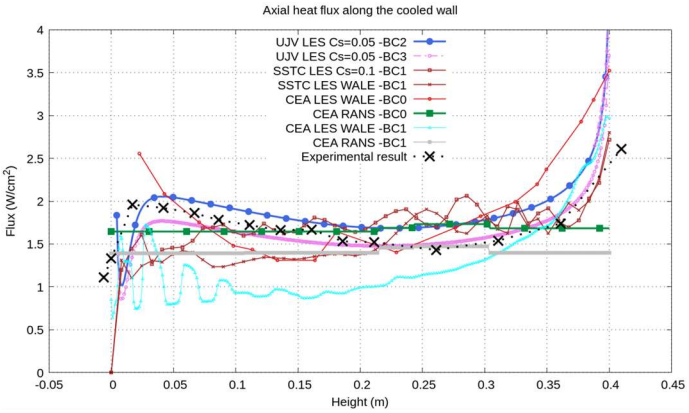

FIGURE 17: Heat flux profile along the cooled wall

Global data on average temperature and heat fluxes support the same conclusions and are not given in this paper for sake of brevity.

6. CONCLUSION

The main safety physical phenomenon in relation to this study is the focusing effect, which is associated with a light metal layer on top of a stratified pool. Indeed, this effect can jeopardize the In-Vessel Retention (IVR) strategy for severe accident mitigation. For IVR strategy to succeed, the heat flux from the Reactor Pressure Vessel to the coolant must remain below the local critical heat flux at all times and points along the vessel. Thus, the light metal layer thermal hydraulic behavior and its associated lateral heat fluxes are of great importance. The global removed lateral heat fluxes have been the subject of many studies in the past and have been correlated to be implemented in macroscopic codes but uncertainties remain on its local behavior especially in regard of the upper light metal pool geometry (thickness over radius ratio). As no prototypical data are available, this study is based on validated CFD solvers associated to adequate CFD schemes in order to simulate the local flow behavior. This benchmark is realized within the framework of the IAEA Coordinated Research Project on In-Vessel Melt Retention. The initial two steps of the methodology have been presented showing the ability of Nek5000, Fluent, ANSYS CFX and TrioCFD to simulate the 5cm height quite laminar BALI-7U and then the 40cm height turbulent BALI-8U test. CFD schemes (boundary conditions, models, meshes) have been discussed. In the future, this work will be pursued by deeper investigation of local flow (frequency of plume detachment, length of the cold tongue), turbulent kinetic energies (TKE), and turbulent heat fluxes (THF). Then following the established benchmark, simulations with liquid steel will be carried out (presenting a lower Prandtl number), possibly in 3D geometry.

ACKNOWLEDGEMENTS

Authors would like to thank the IAEA and the CRP J46002 team. The numerical French work was granted access to the HPC resources of the CEA's Very Large Computing Centre (TGCC) under the allocation 2022 A0092A07691 made by GENCI.

REFERENCES

(Bian et al., 2022) Bian B., Villanueva W., Dovizio D., Direct numerical simulation of molten pool convection in a 3D semicircular slice at different Prandtl numbers, Nuclear Engineering and Design, 393, 111772, 2022.

(Bonnet and Seiler, 1999) Bonnet J.-M., Seiler J.-M., Thermal hydraulic phenomena in corium pools: the BALI experiment, Proc. Int. Conf. Nuclear Engineering ICONE-7057, Tokyo, Japan, 1999.

(Bonnet and Villermaux, 2001) Bonnet J.M., Villermaux C., Assessment of Reactor Vessel Integrity (ARVI) BALI-metal test reports: focusing effect investigation, Report of the 5th Framework progamme on nuclear fission, European Commission, SAM-ARVI-D.2.1.2, 2001.

(Carénini et al., 2020) Carénini et al., Main outcomes from the IVR code benchmark performed in the European IVMR project, Annals of Nuclear Energy 146, 107612, 2020.

(Castaing B., et al., 2006) Castaing B., et al., Scaling of hard thermal turbulence in Rayleigh-Bénard convection, Cambridge University Press, 26 April 2006.

(De et al., 2017) De A.K., Eswaran V., Mishra P.K., Scalings of heat transport and energy spectra of turbulent Rayleigh-Bénard convection in a large-aspect-ratio box, International Journal of Heat and Fluid Flow, 2017.

(Grossmann and Lohse, 2000) Grossmann S. and Lohse D., Scaling in thermal convection: a unifying theory, J. Fluid Mech. (2000), vol. 407, pp. 27–56., 2000

(Le Guennic et al, 2019) Le Guennic C. et al, Study of a thin metal layer: comparison of CFD and integral codes, The 9th European Review Meeting on Severe Accident Research (ERMSAR2019), Prague, Czech Republic, March 2019.

(Le Guennic et al, 2020) Le Guennic C. et al, Synthesis of the WP2.3 results on the metallic layer and new correlations, International Seminar In-vessel retention: outcomes of IVMR project, Palais des Congrès, Juan-les-Pins, France, January 21-22, 2020.

(Li et al., 2021) Li Z., Chang H., Han K., Fang F., Chen L., Experimental investigation on vertical heat transfer characteristics of light metallic layer with low aspect ratio, Nuclear Engineering and Design 377 111153, 2021.

(Lilly, 1992) Lilly D, A proposed modification of the Germano subgrid-scale closure method, Physics of Fluids A 4 633–635, 1992.

(Menter, 1994) Menter, F. R., Two-Equation Eddy-Viscosity Turbulence Models for Engineering Applications. AIAA Journal. 32 (8): 1598–1605, 1994.

(Ma et al., 2015) Ma L., Li J., Ji S., Chang H., Turbulent convection experiment at high Rayleigh number to support CAP1400 IVR strategy, Nuclear Engineering and Design 292 69–75, 2015.

(Nicoud and Ducros, 1999) Nicoud F., Ducros F., Subgrid-scale stress modelling based on the square of the velocity gradient tensor, Flow, Turbulence and Combustion 62, 183–200, 1999.

(Sagaut, 2006) P. Sagaut, Large Eddy Simulation for Incompressible Flows, Springer Science & Business Media, 2006.

(Smagorinsky, 1963) Smagorinsky J., General circulation experiments with the primitive equations I. The basic experiment, Monthly Weather Review 91 99–164, 1963.

 © 2023 by JSME

(Shishkina et al., 2010) Shishkina et al., Boundary layer structure in turbulent thermal convection and its consequences for the required numerical resolution, New J. Phys. 12 075022, 2010

(Theerthan et al., 2020) Theerthan S.A., Kolb G., Sehgal B.R., Heat transfer in internally heated layer with stable stratification induced by phase separation, National Heat Transfer Conference, 2020

(Theofanous et al., 1996) Theofanous, T.G., Liu, C., Additon, S., Angelini, S., Kymäläinen, O., Salmassi, T., In-vessel coolability and retention of a core melt, DOE/ID-10460, vol. 1, 1996.

(Villermaux, 1999) Modélisation physique et numérique de la convection naturelle dans une couche fluide de faible rapport d'aspect dans le cadre des études d'accidents graves de réacteurs à eau sous pression, PhD Thesis, Grenoble, France, 1999. In french.

© 2023 by JSME